Optically driven rotation of exciton-polariton condensates

Yago del Valle Inclan Redondo[1,2], Christian Schneider[3], Sebastian Klembt[4], Sven Höfling[4], Seigo Tarucha[1], and Michael D. Fraser [1,2†]

[1] *RIKEN Center for Emergent Matter Science, Wako-shi, Saitama 351-0198, Japan*

[2] *Physics & Informatics Laboratories (PHI Lab), NTT Research, Inc., Sunnyvale, CA 94085, USA*

[3] *Institute of Physics, University of Oldenburg, D-26129 Oldenburg, Germany*

[4] *Technische Physik, Physikalisches Institut and Wilhelm Conrad Roentgen-Research Center for Complex Material System, Universität Würzburg, Am Hubland, D-97074 Würzburg, Germany*

[†] Corresponding author: michael.fraser@riken.jp

Abstract

The rotational response of quantum condensed fluids is strikingly distinct from rotating classical fluids, especially notable for the excitation and ordering of quantized vortex ensembles. Although widely studied in conservative systems, the dynamics of open-dissipative superfluids such as exciton-polariton condensates remain largely unexplored in this context, as they require high-frequency rotation whilst avoiding resonantly driving the condensate. To address this challenge, we employ a new technique which uses the interference of two off-resonant, frequency-offset laser modes, with two different spatial profiles: Gaussian and Laguerre-Gaussian. The resulting intensity profile has broken axial-symmetry and rotates at the offset frequency. We experimentally demonstrate that this dynamic pump both creates and drives rotation of a spontaneously formed polariton condensate. We directly image and characterize the acquisition of angular momentum with rotation frequencies up to 8 GHz, accompanied by numerical modelling which reveals the crucial role that mechanical and non-Hermitian mechanisms play in driving condensate rotation. The demonstration of this technique enables new opportunities for the study of open-dissipative superfluidity, ordering of non-Hermitian quantized vortex matter, and topological states in a highly non-linear, photonic platform.

Teaser

Using an optical stirrer, we drive rotation of a superfluid of light at GHz frequencies.

Introduction

A defining characteristic of superfluid phases of matter (1) is their unique response to external forces. Subjected to a longitudinal force, the superfluid flow is frictionless below a critical velocity, and under a transverse force, superfluids are irrotational leading to angular momentum being incorporated as phase defects (quantized vortices) above a critical angular momentum (Hess-Fairbank effect) (2). These behaviors are analogous to the phenomena of vanishing resistivity and the expulsion of magnetic fields (Meissner effect) in superconductors, respectively (3). Experimentally, superfluid transport and rotation in particle-conserving platforms has been extensively explored in liquid Helium (4) and dilute-gas atomic Bose-

Einstein condensates (BEC) (5,6). In both cases, rotation is typically induced mechanically, either through rotation of the container in the case of He, or via a stirring laser beam in the case of BEC, with the hallmark in both experiments being the incorporation and self-ordering of quantized vortices with increasing rotation speeds.

Semiconductor microcavity exciton-polaritons, hybrid light-matter quasi-particles, are able to form a Bose-Einstein condensate-like state (7,8) shown to behave as a superfluid (9,10) and to incorporate vortices in their steady-state condensates, either spontaneously from spatial disorder or open-dissipative effects (11-15), in vortex-antivortex lattices with zero total angular momentum (16-19) or nucleated from an initially coherent polariton injection (20-23). More recent work has also explored the possibility of creating and controlling the vortex handedness in optically trapped polariton condensates (24-28), where the non-Hermitian gain-loss landscape drives the mode selection of chiral trapped modes. Although continuous injection of angular momentum has been demonstrated for resonant pumping (23), it is difficult to completely isolate the superfluid response from the phase coherence of the pump laser (29). Continuous driven rotation in a polariton condensate with spontaneous phase coherence is thus highly sought after as it would enable the study of nonlinear pattern formation in vortex matter (6,30), dissipative quantum turbulence (31,32) and the construction of artificial gauge fields (33,34) to realize bosonic quantum Hall effects (6,35-37) in a photonic platform. The main limiting factor has been the high rotational frequencies (100s MHz to GHz) required to generate sufficient angular momentum, due to the very small effective mass of polaritons ($\sim 10^{-5} m_e$) (38).

In this work we used two lasers to create a superposition of a Gaussian and a Laguerre-Gaussian (LG) of orbital charge l (39), with a controllable frequency-offset Δf (Figure 1). Crucially, the resulting intensity pattern is a ring of l holes which possesses a broken axial symmetry (40,41) that can act as a "stirring beam" when off-resonantly injected. An orbital charge of $l = 2$ (azimuthal phase winding of 4π) was used, with the amount of stirring controlled by Δf. This beam was used to pump a GaAs microcavity (see Methods), and by mapping the distribution of flow through imaging photoluminescence we demonstrated the first, continuous incorporation of angular momentum into a spontaneously formed polariton condensate.

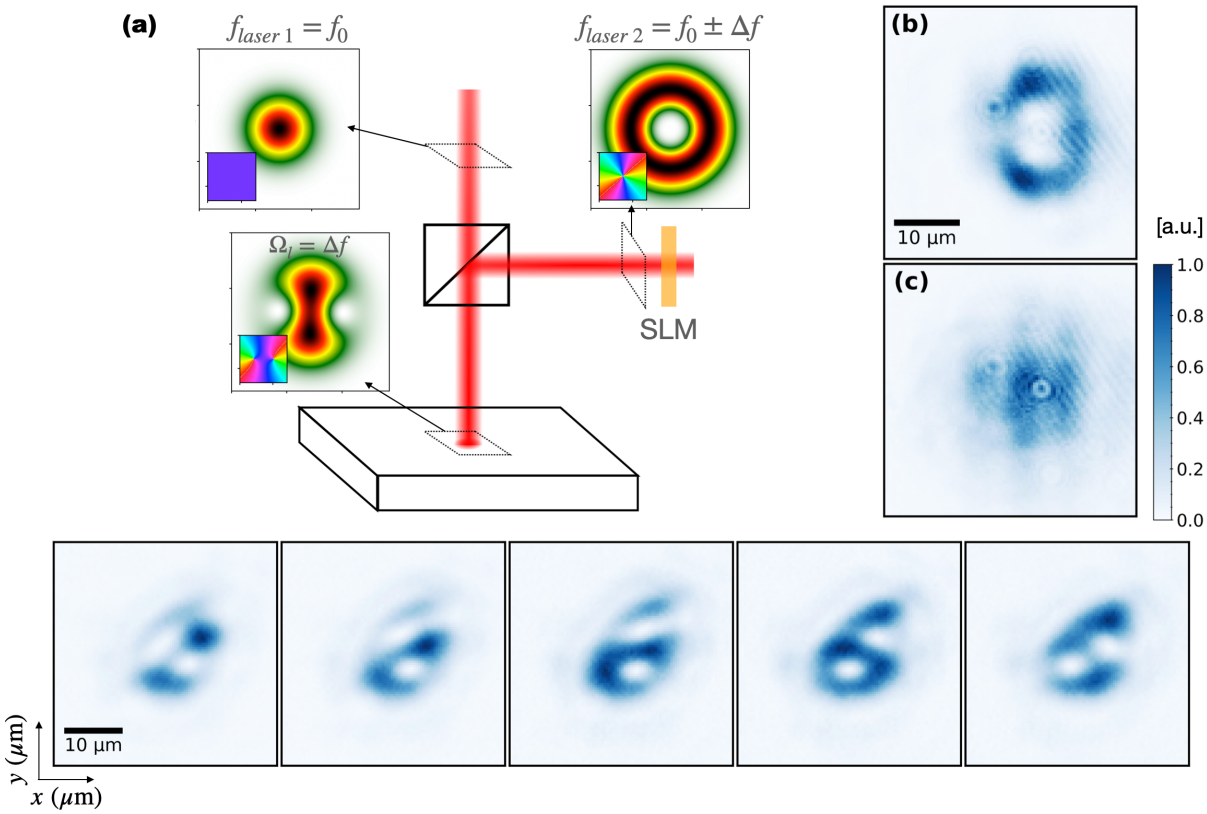

Figure 1: *A rotating pump is formed by the coherent superposition of a Gaussian and an* $l = 2$ *Laguerre-Gauss mode with a frequency offset of* Δf*. (a) Simplified schematic of pumping process with numerically calculated intensity and phase (inset) of each pump laser and their superposition. Experimental measurements of the (b) LG and (c) Gaussian modes on the microcavity sample surface and (d) a series of temporal snapshots of the experimental rotating superposition profile.*

Results

A confocal microscopy setup (see Methods) is used to map the direction and magnitude of condensate flow at all points in space, allowing the detection of azimuthal flow as the hallmark of rotation (Fig. 2a). A pinhole aperture filters emission at given spatial location (Fig. 2b), which is then imaged in momentum space with the centroid of the resulting cloud corresponding to the average momentum of polaritons at that position. As expected for a pinhole at $x > 0$, the cloud centroid is shifted to $k_x > 0$ (Fig. 3c) from the radial expansion (42,43) that arises from nonlinear interaction with the nonresonant pump. To distinguish rotation-induced flow from this radial expansion and from sample or pump spatial inhomogeneity, we carry out a differential measurement between momentum clouds of

condensates rotating at the same frequency but with opposite handedness. At low frequency ($|\Delta f| = 20$ MHz, Fig. 2d), the deflection of the condensate momentum cloud is small ($\sim 1\%$) and has a spatial structure that varies with sample position. At high frequency ($|\Delta f| = 3$ GHz, Fig. 2c,e), a transverse shift of the momentum cloud is observed, appearing as two distinct lobes in the map of differential density which are robust to movements in sample position. This demonstrates that the rotating pump overcomes sample disorder and creates transverse flow in the condensate. Spatially scanning the position of the pinhole shows that the differential flow at high frequency is azimuthal (Fig. 2f) confirming that the entire condensate is experiencing rotation and incorporating angular momentum from the nonresonant pump.

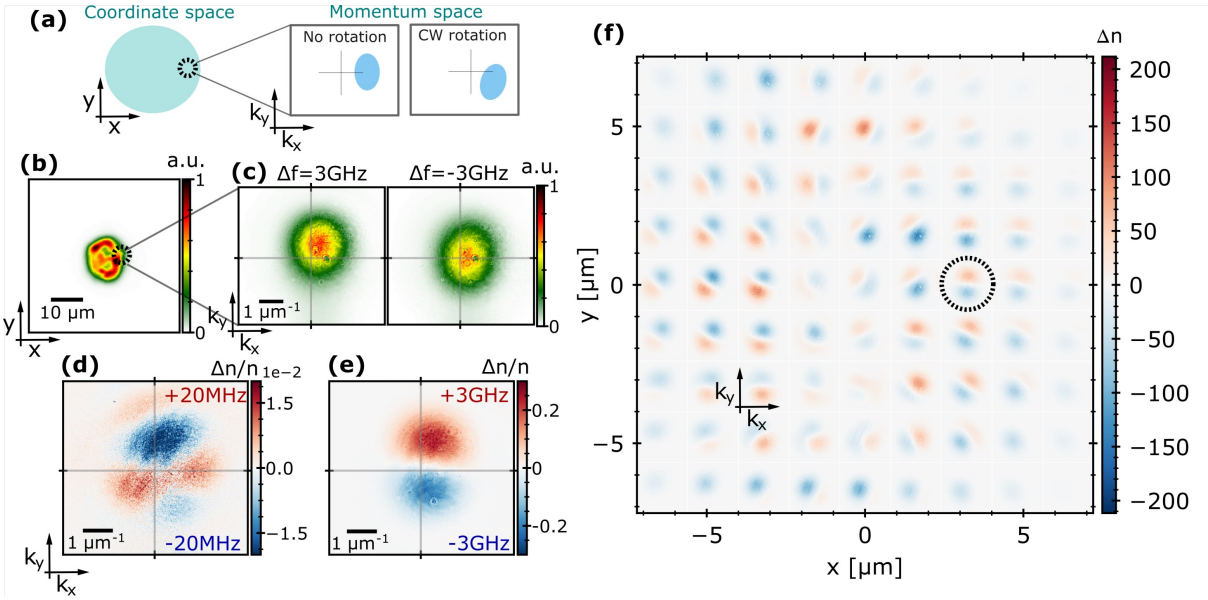

Figure 2: Differential measurement of condensate rotation. *(a) Schematic of expected momentum-space clouds for spatially filtered, non-rotating and rotating condensates. (b) Real-space condensate density distribution and (c) measured momentum-space clouds of spatially filtered (black dashed circle) condensate emission for $\Delta f = \pm 3$ GHz. (d) Differential density map at $\Delta f = \pm 20$ MHz. (e) and at $\Delta f = \pm 3$ GHz (from data in panel c). (f) Combined differential density maps for a spatially scanned aperture. Measurement in (e) is circled.*

Condensate rotation and its dependency on frequency is further quantified by constructing vector flow maps and estimating their angular momentum (see Methods). Momentum flow maps (Fig. 3a,b) show that the handedness of azimuthal flow is controlled by the direction of pump rotation. Sample and pump inhomogeneities lead to an asymmetric rotational response with respect to rotation direction, resulting in negative frequencies having more disordered

flow (Fig. 3a) and the center of the rotation not being identical at different frequencies. Nonetheless, the correlation between the handedness of the pump rotation and of the condensate angular momentum is conclusive (Fig. 3c,d). Additionally, for condensates with higher angular momentum ($\Delta f = 5$ GHz) azimuthal flow is concentrated away from the axis of rotation suggesting that divergent flows of the unconfined condensate are limiting the incorporation of angular momentum (this idea is further explored in the Discussion). Finally, the total condensate angular momentum per particle ($l = L/N$) also has a handedness consistent with that of the pump at all values of Δf (Fig. 3e). At large positive frequencies, l is found to saturate at $\sim 0.3\hbar$, below the angular momentum of a single on-axis vortex, i.e. $l = 1\hbar$, consistent with our lack of vortex signatures in interferometry measurements (see Supplementary Information). This is analogous to a trapped rotating atomic BEC, where small values of angular momentum are incorporated by center of mass motion and surface waves, with quantized vortices only appearing above a critical rotation speed (38).

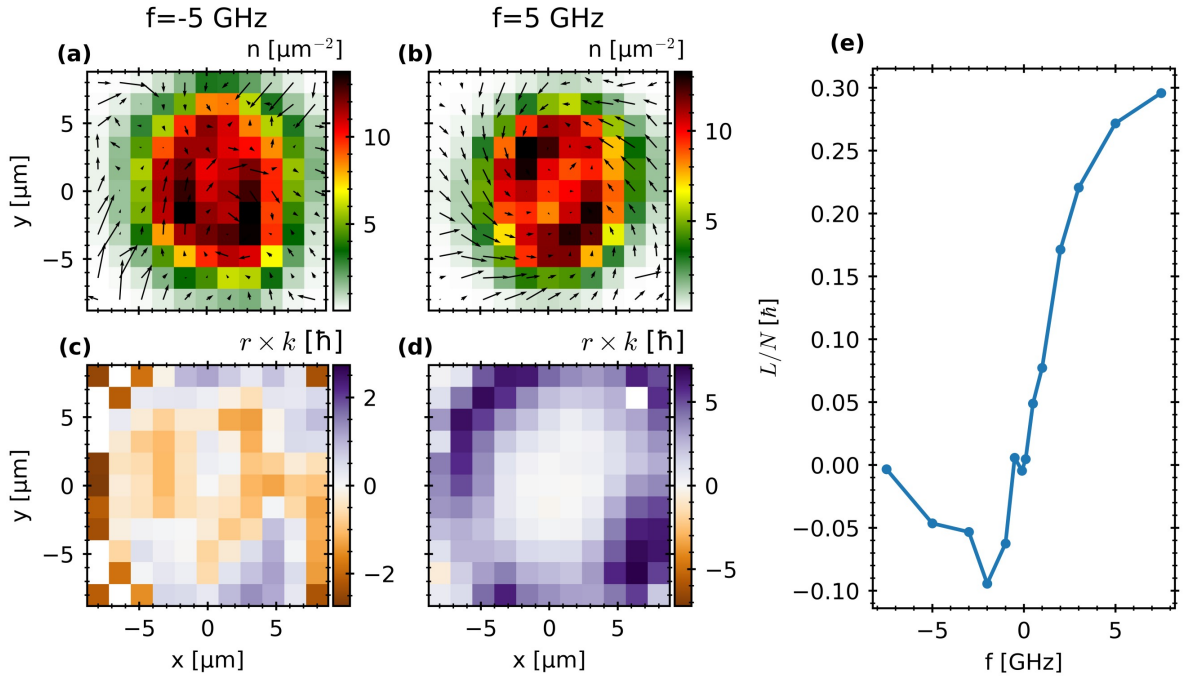

***Figure 3: Frequency dependence of condensate rotation**. (a,b) Condensate density and rotation-induced velocity map extracted from spatially pin-holed data at two different rotation frequencies. (c,d) Angular momentum distribution of the velocity maps in (a,b). (e) Angular momentum per particle $l = L/N$ across the measurement area as a function of pump rotation frequency.*

To determine the mechanism of optical rotation of the polariton condensate, and to explain the values of angular momentum observed, numerical solutions of an open-dissipative Gross-Pitaevskii model (44) (see Methods) are compared with experimental results. Using a pump profile and polariton properties applicable to the experiment, condensate rotation is found over a wide range of parameters, all with a consistent rotation mechanism. For a rotation speed of $\Delta f = 10\ \mathrm{GHz}$, simulations show that the time-integrated condensate density and vector flow map (Fig 4a), spatial distribution of transverse flow magnitude (Fig 4b) and accumulation of angular momentum with increasing pump rotation velocity (Fig 4c), all have a close qualitative match to the experimental data in Figures 3b,d,e respectively. Notably, the simulations accurately capture the inwardly directed flow at the condensate center and angular momentum build-up away from the rotation axis (Fig. 4a,b) and the monotonic increase and saturation of the angular momentum per particle (Fig. 4c, blue curve) with agreement on its magnitude.

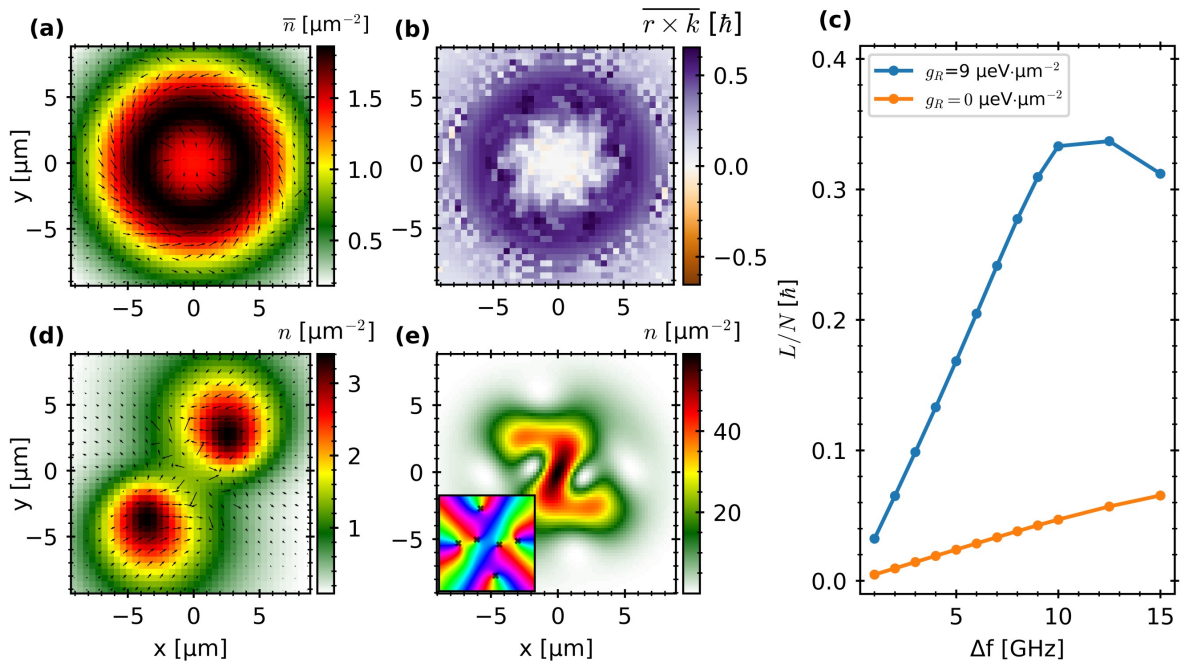

Figure 4: Numerical simulations of rotating condensate dynamics*. (a) Average condensate density with rotation-induced momentum map, and (b) spatial distribution of average angular momentum for a $\Delta f = 10\ \mathrm{GHz}$ rotating pump. (c) Total angular momentum per particle $l = L/N$ as a function of pump rotation frequency for two values of condensate-reservoir interaction coefficient g_R (see Methods). (d) Instantaneous condensate density and rotation-induced momentum map from (a). (e) Instantaneous condensate density under the same parameters as (d) with a confining potential additionally applied. Inset shows the condensate phase with vortex positions indicated.*

Individual temporal frames show that the spatially inhomogeneous pump generates a condensate profile which, for the $l = 2$ pump superposition, specifically forms a two-lobed structure (Fig. 4d). This profile is largely the consequence of repulsive interactions between the condensate and the reservoir causing spatial overlap to be minimized. Additionally, pump rotation causes the condensate profile to become asymmetric about the azimuthal coordinate, a condition which is continuously maintained as the pump and reservoir rotate, thus driving a net non-zero angular momentum. The spatially structured, time-dependent gain and loss also influence the condensate profile and its rotation, which we numerically demonstrate by setting the condensate-reservoir interaction coefficient to zero (orange line Fig. 4c, see Supplementary Information). The condensate still acquires increasing angular momentum as the frequency is increased, but the total magnitude is significantly reduced. Thus, while mechanical stirring by the reservoir and non-Hermitian gain-loss dynamics both contribute to the condensate rotation, the former dominates in these experiments. For both mechanical and non-Hermitian stirring however, as the pump rotation speed is increased the condensate distribution along the azimuthal coordinate becomes more asymmetric, leading to larger angular momentum.

Finally, to confirm our assumption that the incorporation of sufficient amounts of angular momentum to nucleate quantized vortices is suppressed by the lack of radial confinement, we add a $12\ \mu\mathrm{m}$ radius, hard-walled trapping potential to the simulations. The external potential largely suppresses the Magnus forces (45) present in the inhomogeneous condensate which radially repel vortices away from high density regions (46). The $\Delta f = 10\ \mathrm{GHz}$ pump rotation frequency is estimated to be sufficient to nucleate quantized vortices, and Fig 4e shows that while the inhomogeneous pump still creates a non-uniform condensate, numerous quantized vortices are now nucleated, stabilized, and develop some degree of order. The angular momentum per particle is $\sim 5\times$ that of the identical parameters without a trapping potential in Fig 4d.

Discussion

We have reported the first continuous, off-resonant injection of angular momentum into an exciton-polariton condensate, using a rapidly rotating optical pump. Evidence for driven rotation is obtained by spatially mapping the condensate flow and characterizing the angular momentum, finding that the condensate responds to the rotating pump up to frequencies of $8\ \mathrm{GHz}$ with flow direction controlled by the handedness of the pump. The physics responsible for these phenomena is found to be driven predominantly by mechanical stirring induced by a thermal reservoir, with a smaller role played by non-Hermitian dynamics. Angular momentum is measured up to $\sim 0.3\hbar$/particle, where steady-state vortices are not easily incorporated due to the lack of a confining potential. With the addition of a trapping potential however, simulations show that this technique is capable of injecting large amounts of angular momentum and nucleating numerous vortices. Our demonstration of a scheme to generate a fast-rotating condensate without coherent imprinting opens up numerous opportunities for study of superfluidity and quantized vortex ordering in an open-dissipative condensate and will lead to new ways of generating topological photonic matter in a highly non-linear and controllably non-Hermitian platform.

Methods

Semiconductor microcavity sample – The microcavity sample used consists of 27(23) AlAs/$Al_{0.2}Ga_{0.8}As$ mirror pairs for the bottom(top) distributed Bragg reflectors (DBRs) forming a λ/2 cavity with 3 sets of 4 × 13 nm wide GaAs/AlAs QWs, one set placed at the anti-node of the cavity and one set in each of the two first mirror pairs. The Rabi splitting is $2\hbar\Omega \approx 6.7\ \mathrm{meV}$.

Lasers – Two low-noise lasers are used: a cavity-stabilized Spectra-Physics Matisse CW Ti:Sapphire (time-averaged linewidth $< 200\ \mathrm{kHz}$) and a Toptica tapered fiber amplifier (typical linewidth $\sim 50\ \mathrm{kHz}$). A small fraction (<5%) of each beam is picked off, combined, and filtered through a single-mode fiber, with resulting temporal interference measured on a fast photodiode. The beat signal is used to monitor and manually tune the frequency offset of the Toptica from the Matisse ($|\Delta f| < 10\ \mathrm{GHz}$). A simple fork pattern on a Hamamatsu X-10468 spatial light modulator converts the Matisse laser into a LG mode of tunable charge. The two

lasers are merged with a beam-splitter and put through a 20x objective to pump the sample. An LG orbital charge of $l = 2$ was chosen to create a reflection-symmetric modulation around the center whilst minimizing diffraction losses at the spatial-light modulator. The resulting mode consists of $l = 2$ holes distributed on a ring with a radius determined by the relative amplitude of the two constituent modes. Both lasers are tuned to the first Bragg minimum of the microcavity, corresponding to a wavelength of $\lambda_{pump} \sim 760\ \mathrm{nm}$. The spectral width of the first Bragg minimum is $\Delta\lambda \sim 0.85\ \mathrm{nm}$, significantly broader than the maximum used $20\ \mathrm{GHz}$ scanning range ($\sim 0.02\ \mathrm{nm}$) of the Toptica.

Experimental apparatus - Photoluminescence imaging measurements are conducted in a continuous-flow liquid helium cryostat, maintaining a fixed sample temperature of 4 K. A 100 Hz mechanical chopper with 10% duty cycle is used to modulate the pumping beam and limit sample heating. We utilize two sets of confocal optics to allow access to both the spatial and momentum coordinate Fourier planes, in addition to giving independent control over the resolution and field of view in both coordinate spaces on the imaging camera. Figure 5 shows a simplified schematic of the imaging optics.

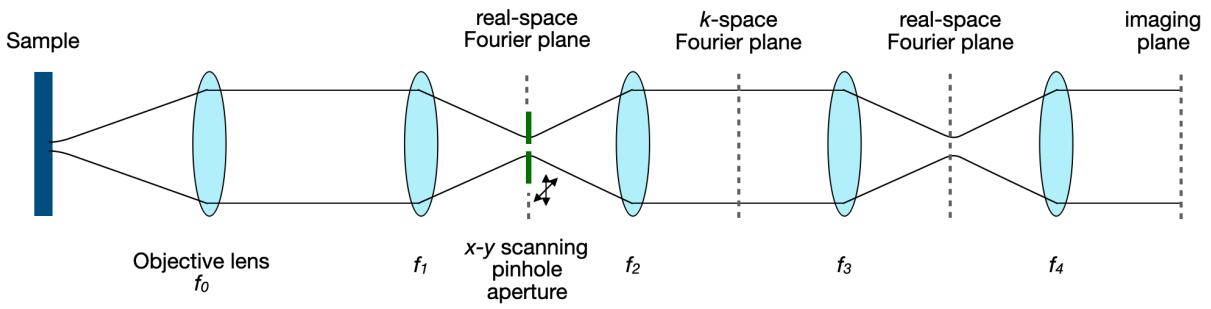

Figure 5: *Simplified schematic of confocal imaging optics setup, highlighting the positions of Fourier space planes and the scanning pin-hole aperture in the first real-space plane.*

To resolve the polariton momentum vector, a pinhole aperture is scanned in the spatial Fourier plane of the confocal optics setup. The average momentum at that pinhole position is then taken to be the centroid of the photoluminescence cloud in momentum space. The pinhole diameter of $100\ \mu\mathrm{m}$ (~1.6 $\mu\mathrm{m}$ on the sample) is chosen to optimize the light throughput and balance the resolutions in the conjugate spatial and momentum coordinates.

Numerical simulations - The two-dimensional condensate dynamics are numerically simulated using the open-dissipative Gross-Pitaevskii equation (ODGPE) (7), forms of which have been used extensively in studies exciton-polariton excitations and dynamics (8). This set of two coupled equations, Eqs. (4)-(5) describe the time-dependent dynamics of a condensed bosonic state $\psi(\boldsymbol{r},t)=\sqrt{n_C(\boldsymbol{r},t)}e^{i\phi(\boldsymbol{r},t)}$ of lower polaritons (LP) (eq. 1) coupled to a reservoir of thermal polaritons $n_R(\boldsymbol{r},t)$ (eq. 2):

$$i\hbar\frac{\partial\psi(\boldsymbol{r},t)}{\partial t}=\left(-\frac{\hbar^2\nabla^2}{2M}+V_E(\boldsymbol{r})-\frac{i\hbar}{2}\left[\gamma_C-Rn_R(\boldsymbol{r},t)\right]+g_{2D}|\psi(\boldsymbol{r},t)|^2+g_Rn_R(\boldsymbol{r},t)\right)\psi(\boldsymbol{r},t) \tag{1}$$

$$\frac{\partial n_R(\boldsymbol{r},t)}{\partial t}=P_l(\boldsymbol{r},t)-\gamma_Rn_R(\boldsymbol{r},t)-Rn_R(\boldsymbol{r},t)|\psi(\boldsymbol{r},t)|^2 \tag{2}$$

$P_l(\boldsymbol{r},t)$ is the rotating pump. Fixing the polariton mass and lifetime, and condensate size with those extracted from experiments, the polariton non-linearity, reservoir lifetime and scattering rate are varied for a qualitive match to experimental measurements. Typical parameters used in these simulations are LP effective mass $M\sim5\times10^{-5}m_e^0$ (m_e^0 is the free electron mass), LP decay rate $\gamma_C\sim0.2\ \mathrm{ps}^{-1}$, reservoir decay rate $\gamma_R\sim0.1\ \mathrm{ps}^{-1}$, stimulated scattering rate $R\sim0.03\ \mu\mathrm{m}^2\cdot\mathrm{ps}^{-1}$, condensate self-interaction $g_C\sim4.5\ \mu\mathrm{eV}\cdot\mu\mathrm{m}^{-2}$ and condensate-reservoir interaction $g_C=2g_R$. The external potential $V_E(\boldsymbol{r})$ is 0, except for the data in Fig 4e, where $12\ \mu\mathrm{m}$ radius hard-wall trap is used. This set of equations is solved using the split-step operator method.

References

1. L. Pitaevskii and S. Stringari, 'Bose-Einstein condensation and superfluidity' Oxford University Press (2016).
2. G. B. Hess, and W. M. Fairbank 'Measurements of angular momentum in superfluid helium' Phys. Rev. Lett., **19**, 216. (1967).

3. D. R. Tilley and J. Tilley, 'Superfluidity and superconductivity'. Routledge. (1990).

4. E. J. Yarmchuk, M. J. V. Gordon and R. E. Packard. 'Observation of stationary vortex arrays in rotating superfluid helium.' Phys. Rev. Lett. **43** 214 (1979)

5. C. Raman, J. R. Abo-Shaeer, J. M. Vogels, K. Xu and W. Ketterle, 'Vortex Nucleation in a Stirred Bose-Einstein Condensate' Phys. Rev. Lett. **87**, 210402 (2001).

6. A. L. Fetter, 'Rotating Trapped Bose-Einstein Condensates' Rev. Mod. Phys. **81**, 647 (2009).

7. H. Deng, H. Haug, and Y. Yamamoto, 'Exciton-polariton Bose-Einstein condensation' Rev. Mod. Phys. **82**, 1489 (2010).

8. I. Carusotto and C. Ciuti, 'Quantum fluids of light' Rev. Mod. Phys. **85**, 299 (2013).

9. A. Amo, J. Lefrère, S. Pigeon, C. Adrados, C. Ciuti, I. Carusotto, R. Houdré, E. Giacobino and A. Bramati 'Superfluidity of polaritons in semiconductor microcavities' Nat. Phys. **5**, 805 (2009)

10. G. Lerario, A. Fieramosca, F. Barachati, D. Ballarini, K. S. Daskalakis, L. Dominici, M. De Giorgi, S. A. Maier, G. Gigli, S. Kéna-Cohen and D. Sanvitto 'Room-temperature superfluidity in a polariton condensate' Nat. Phys. **13**, 837 (2017)

11. K. G. Lagoudakis, M. Wouters, M. Richard, A. Baas, I. Carusotto, R. André, Le Si Dang and B. Deveaud-Plédran, 'Quantized vortices in an exciton–polariton condensate' Nat. Phys. **4**, 706 (2008).

12. K. G. Lagoudakis, T. Ostatnickỳ, A. V. Kavokin, Y. G. Rubo, R. André and B. Deveaud-Plédran, 'Observation of half-quantum vortices in an exciton-polariton condensate' Science **326**, 974 (2009).

13. G. Roumpos, M. D. Fraser, A. Löffler, S. Höfling, A. Forchel and Y. Yamamoto, 'Single vortex-antivortex pair in an exciton-polariton condensate' Nature Physics **7**, 129–133 (2010)

14. J. Keeling and N. G. Berloff, 'Spontaneous rotating vortex lattices in a pumped decaying condensate' Phys. Rev. Lett. **100**, 250401 (2008).

15. M. O. Borgh, G. Franchetti, J. Keeling and N. G. Berloff, 'Robustness and observability of rotating vortex lattices in an exciton-polariton condensate' Phys. Rev. B **86**, 035307 (2012).

16. T.C.H. Liew, Y. G. Rubo and A. V. Kavokin, 'Generation and dynamics of vortex lattices in coherent exciton-polariton fields' Phys. Rev. Lett. **101**, 187401 (2008).

17. A. V. Gorbach, R. Hartley and D. V. Skryabin, 'Vortex lattices in coherently pumped polariton microcavities' Phys. Rev. Lett. **104**, 213903 (2010).

18. G. Tosi, G. Christmann, N. G. Berloff, P. Tsotsis, T. Gao, Z. Hatzopoulos, P. G. Savvidis and J. J. Baumberg, 'Geometrically locked vortex lattices in semiconductor quantum fluids' Nat. Comm. **3**, 1 (2012).

19. R. Hivet, E. Cancellieri, T. Boulier, D. Ballarini, D. Sanvitto, F. M. Marchetti, M. H. Szymanska, C. Ciuti, E. Giacobino, and A. Bramati 'Interaction-shaped vortex-antivortex lattices in polariton fluids' Phys. Rev. B **89**, 134501 (2014)

20. D. Sanvitto, F. M. Marchetti, M. H. Szymańska, G. Tosi, M. Baudisch, F. P. Laussy, D. N. Krizhanovskii, M. S. Skolnick, L. Marrucci, A. Lemaître, J. Bloch, C. Tejedor and L. Viña, 'Persistent currents and quantized vortices in a polariton superfluid' Nat. Phys. **6**, 527 (2010).

21. L. Dominici, R. Carretero-González, A. Gianfrate, J. Cuevas-Maraver, A. S. Rodrigues, D. J. Frantzeskakis, G. Lerario, D. Ballarini, M. De Giorgi, G. Gigli, P. G. Kevrekidis and D. Sanvitto, 'Interactions and scattering of quantum vortices in a polariton fluid' Nat. Comm. **9**, 1 (2018).

22. D. Caputo, N. Bobrovska, D. Ballarini, M. Matuszewski, M. De Giorgi, L. Dominici, K. West, L. N. Pfeiffer, G. Gigli and D. Sanvitto 'Josephson vortices induced by phase twisting a polariton superfluid' Nat. Phot. **13**, 488 (2019)

23. T. Boulier, E. Cancellieri, N. D. Sangouard, Q. Glorieux, A. V. Kavokin, D. M. Whittaker, E. Giacobino and A. Bramati, 'Injection of orbital angular momentum and storage of quantized vortices in polariton superfluids' Phys. Rev. Lett. **116**, 116402 (2016).

24. R. Dall, M. D. Fraser, A. S. Desyatnikov, G. Li, S. Brodbeck, M. Kamp, C. Schneider, S. Höfling, and E. A. Ostrovskaya, 'Creation of orbital angular momentum states with chiral polaritonic lenses' Phys. Rev. Lett. **113**, 200404 (2014).

25. T. Gao, G. Li, E. Estrecho, T. C. H. Liew, D. Comber-Todd, A. Nalitov, M. Steger, K. West, L. Pfeiffer, D. Snoke, A. V. Kavokin, A. G. Truscott, E. A. Ostrovskaya, 'Chiral modes at exceptional points in exciton-polariton quantum fluids' Phys. Rev. Lett. **120**, 065301 (2018).

26. X. Ma, B. Berger, M. Aßmann, R. Driben, T. Meier, C. Schneider, S. Höfling and S. Schumacher 'Realization of all-optical vortex switching in exciton-polariton condensates' Nat. Comm. **11**, 897 (2020)

27. M-S. Kwon, B. Y. Oh, S-H. Gong, J-H. Kim, H. K. Kang, S. Kang, J. D. Song, H. Choi and Y-H. Cho, 'Direct Transfer of Light's Orbital Angular Momentum onto a Nonresonantly Excited Polariton Superfluid' Phys. Rev. Lett. **122**, 045302 (2019).

28. D. Choi, M. Park, B. Y. Oh, M.-S. Kwon, S. I. Park, S. Kang, J. D. Song, D. Ko, M. Sun, I. G. Savenko, Y.-H. Cho and H. Choi 'Observation of a single quantized vortex vanishment in exciton-polariton superfluids' Phys. Rev. B **105**, L060502 (2022)

29. R. T. Juggins, J. Keeling and M. H. Szymańska 'Coherently driven microcavity-polaritons and the question of superfluidity' Nat. Comm. **9**, 4062 (2018)

30. T.L. Ho, 'Bose-Einstein Condensates with Large Number of Vortices', Phys. Rev. Lett. **87**, 60403 (2001).

31. S.V.Koniakhin, O.Bleu, G.Malpuech, D.D.Solnyshkov, '2D quantum turbulence in a polariton quantum fluid' Chaos, Solitons & Fractals **132**, 109574 (2020)

32. J. A. Estrada, M. E. Brachet and P. D. Mininni 'Turbulence in rotating Bose-Einstein condensates' Phys. Rev. A 105, 063321 (2022)

33. M. C. Rechtsman, J. M. Zeuner, Y. Plotnik, Y. Lumer, D. Podolsky, F. Dreisow, S. Nolte, M. Segev and A. Szameit 'Photonic Floquet topological insulators' Nature **496**, 196 (2013)

34. M. Aidelsburger, S. Nascimbene and N. Goldman, 'Artificial gauge fields in materials and engineered systems' Comptes Rendus Physique **19**, 394 (2018).

35. N. K. Wilkin and J. M. F. Gunn, 'Condensation of "composite bosons" in a rotating BEC' Phys. Rev. Lett. **84**, 6 (2000).

36. N. Schine, A. Ryou, A. Gromov, A. Sommer and J. Simon, 'Synthetic Landau levels for photons' Nature **582**, 41 (2020).

37. L. W. Clark, N. Schine, C. Baum, N. Jia and J. Simon, 'Observation of Laughlin states made of light' Nature **582**, 41 (2020).

38. C. J. Pethick and H. Smith, 'Bose-Einstein Condensation in Dilute Gases' Cambridge University Press (2008)

39. L. Allen, S. M. Barnett and M. J. Padgett, 'Optical angular momentum' CRC Press (2016).

40. S. Franke-Arnold, J. Leach, M. J. Padgett, V. E. Lembessis, D. Ellinas, A. J. Wright, J. M. Girkin, P. Ohberg and A. S. Arnold, 'Optical ferris wheel for ultracold atoms' Optics Express **15**, 8619 (2007).

41. Y. V. Kartashov and D. A. Zezyulin, 'Rotating patterns in polariton condensates in ring-shaped potentials under a bichromatic pump', Opt. Lett. **44**, 4805 (2019)

42. M. Wouters, I. Carusotto and C. Ciuti, 'Spatial and spectral shape of inhomogeneous nonequilibrium exciton-polariton condensates' Phys. Rev. B **77**, 115340 (2008)

43. G. Christmann, G. Tosi, N. G. Berloff, P. Tsotsis, P. S. Eldridge, Z. Hatzopoulos, P. G. Savvidis, and J. J. Baumberg 'Polariton ring condensates and sunflower ripples in an expanding quantum liquid' Phys. Rev. B 85, 235303 (2012)

44. M. Wouters and I. Carusotto, 'Excitations in a nonequilibrium Bose-Einstein condensate of exciton polaritons' Phys. Rev. Lett. **99**, 140402 (2007).

45. E.B. Sonin, 'Magnus force in superfluids and superconductors' Phys. Rev. B **55**, 485-501 (1997).

46. M. D. Fraser, G. Roumpos and Y. Yamamoto 'Vortex–antivortex pair dynamics in an exciton–polariton condensate' New J. Phys. **11** 113048 (2009).

47. H. Ohadi, A. Dreismann, Y. G. Rubo, F. Pinsker, Y. del Valle-Inclan Redondo, S. I. Tsintzos, Z. Hatzopoulos, P. G. Savvidis and J. J. Baumberg 'Spontaneous Spin Bifurcations and Ferromagnetic Phase Transitions in a Spinor Exciton-Polariton Condensate' Phys. Rev. X **5**, 031002 (2015).

Acknowledgements

The authors acknowledge financial support by the Japan Society for the Promotion of Science Grants-in-Aid for Scientific Research (JSPS KAKENHI) Grant Numbers JP17H04851 and JP19H0561, the Japan Science and Technology Agency (JST) PRESTO Grant Number JPMJPR1768, NTT Research and the State of Bavaria.

Author contributions

M.D.F. conceived the project and carried out the numerical simulations. Y.dVI.R. conducted the experiments and analyzed the data. M.D.F. and Y.dVI.R. constructed the experimental apparatus, interpreted the data, and wrote the paper. C.S., S.K. and S.H. prepared the samples. All authors contributed to discussions and to the final manuscript.

Competing Interests

The authors declare that they have no competing interests.

Data availability

All data needed to evaluate the conclusions in the paper are present in the paper and/or the Supplementary Materials.